

Muscle-Like Soft Actuation for Motor-Less Robotic Exoskeletons

Julian D. Colorado¹^a, John E. Bermeo¹^b, Fredy A. Cuellar¹^c, Catalina Alvarado-Rojas¹^d,
Diego Mendez¹^e, Angela M. Iragorri²^f and Ivan F. Mondragon¹^g

¹*School of Engineering, Pontificia Universidad Javeriana, Bogota, 110231, Colombia*

²*Neurology, School of Medicine, Hospital Universitario San Ignacio, Bogota, 110231, Colombia*

Keywords: Shape Memory Alloys, Exoskeletons, Soft Actuation, Rehabilitation Robotics.

Abstract: Shape Memory Alloys (SMAs) have opened new alternatives upon conventional actuation technologies used in robotics. SMA-based actuators are also known as muscle-like actuation mechanisms, in which Nickel titanium (Nitinol) fibers operate as artificial tendons for soft actuation. This paper explores the use and limits of tendon-like SMA actuation for a robotic exoskeleton to actively support hand motion rehabilitation.

1 INTRODUCTION

Actuation technology based on smart materials has opened new alternatives in robotics systems. Piezoelectric fiber composites (Mishra, 2022), electroactive polymers (Hodgins, 2014) and shape memory alloys (Guo, 2015; Bhatt, 2022) are being adopted to replace classical servomotor actuators, enabling a new generation of soft robotic applications (Jeong, 2023; Jin, 2016).

In particular, shape memory alloys (SMA) are an interesting alternative to developing bio-inspired actuation mechanisms, by mimicking the way how muscles generate motion in several biological organisms, with the advantage of reducing the size and weight of the system, while obtaining higher force-weight ratio and precise sensing capabilities. In this regard, SMAs have opened new alternatives and the potential of building lighter and smaller soft robotic systems for motor rehabilitation (Stano, 2021; Wang, 2020).


In this arena, robotic exoskeletons are being actively applied to support the activities of daily living (ADLs) for patients with motion impairments. In this regard, SMAs have been used in exoskeletons for rehabilitation, by applying additive manufacturing ap-


proaches (Stano, 2021). Additionally, bio-mimetic systems using SMAs (Wang, 2020) are playing an important role for modeling and controlling human hand kinematics without the restrictions of rigid mechanical joints, while having an entire deformable body with limitless points of actuation (Wang, 2022). In this regard, closed-loop position and velocity controllers can be developed to regulate SMA operation precisely (Ruth, 2022; Singh, 2022; Khan, 2022). However, issues such as the power consumption and control bandwidth are the main limits of this technology.


This paper proposes the application of tendon-like SMA actuation for a robotic exoskeleton mechanics model developed in prior work reported in (Castiblanco, 2021). The ultimate goal is to migrate our current heavy and bulky rigid-body mechanism to a softer and lighter prototype, by including these muscle-like SMA actuators. Here, we demonstrate the functionality and accuracy of this technology applied to our exoskeleton model, allowing to conclude on the future research directions to be tackled in order to overcome the inherent drawbacks when using bio-inspired soft actuation for robotic-aided rehabilitation tasks.


2 METHODS


SMA wires can be mechanically connected to a joint to generate rotational motion during the contraction of the NiTi alloys upon heating. In order to achieve two-


^a <https://orcid.org/0000-0002-6925-0126>


^b <https://orcid.org/0000-0001-7183-4027>

^c <https://orcid.org/0009-0003-2261-1654>

^d <https://orcid.org/0000-0002-2315-5692>

^e <https://orcid.org/0000-0002-9866-4416>

^f <https://orcid.org/0000-0002-0249-4951>

^g <https://orcid.org/0000-0002-7828-6681>

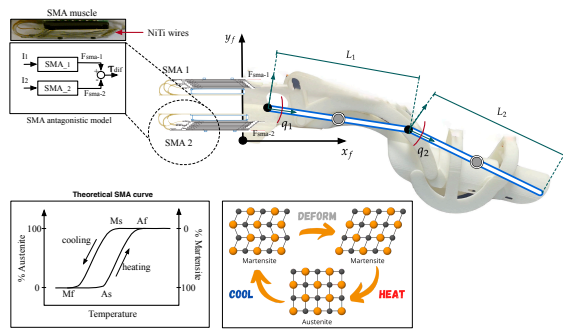


Figure 1: SMA-driven exoskeleton finger testbed. Artificial muscles are placed by following an antagonistic configuration. Each finger is modeled as a serial chain composed by 2 DoF links. The joint q_1 is directly actuated by the SMA actuators, according to the pull forces F_{sma1} and F_{sma2} , whereas q_2 is an underactuated joint. The insets below elucidate the theoretical curve of SMA NiTi alloys for each phase transformation: Austenite and Martensite.

way rotational motion, a biasing returning force must be induced. To this purpose, we propose an antagonistic arrangement of SMA actuators, as shown in Fig 1. We used the commercial nanomuscle model NM706-Super manufactured by MigaMotors, consisting of 6 Nickel titanium (NiTi) wires stacked in parallel, with an overall mass of 1.1g and stroke of 4mm.

In this paper, we present how to use SMA thermo-mechanical phenomenological equations to elucidate the martensitic transformation between the high temperature austenite phase and the low temperature martensite stage of the NiTi alloys. This allows to evaluate and explore the limits of SMA operation in terms of actuation frequency and output range of motion, by keeping the input power below the limits of SMA wire overheating. Figure 1 introduces the proposed muscle-like SMA driven exoskeleton.

2.1 SMA-Driven Muscle-Like Actuation

The exoskeleton can assist in both open and close finger gestures, since both directions can be actively controlled. However, it is crucial to have an understanding of the SMA hysteresis curve, in order to evaluate the proposed antagonistic configuration.

Tanaka in (Tanaka, 1986) presented one of the first approaches to study NiTi SMA behavior, by using a dimensional thermo-mechanical model based on a stress-induced input. Elahinia et al. (Elahinia, 2005), complemented Tanaka's model by extending the equations to support electrical stimulation, and by connecting the effects of electrical current input with alloy temperature and stress, while taking into account the two-way shape memory effect. In our application, the exoskeleton mechanics and the pa-

tient's hand will impose a significant external payload to the SMA actuation system, requiring characterization to determine the limits of SMA operation. In previous work reported in (Colorado, 2012; Coral, 2012), SMAs were experimentally characterized in terms of the power-to-force ratio, using muscle-like actuation to drive a bio-inspired fish robot and bat-like aerial vehicle with morphing wings. Here, we used similar approaches for both modeling and control, by applying the Elahinia's SMA model, which consists in several equations described in Algorithm 1.

Algorithm 1: SMA thermo-mechanical computation.

1. Compute SMA temperature rate:

$$\dot{T} \leftarrow m_{sma}^{-1} c_p^{-1} (i^2 R_{sma} - h_c A_c (T - T_o))$$
2. Calculate the SMA stress rate upon heating:

$$\dot{\sigma} \leftarrow \frac{\theta_s - \Omega(A_f - A_s)^{-1}}{1 - \Omega(A_f - A_s)^{-1} C_m} \dot{T}$$
3. Calculate phase transformation rate:

$$\dot{\xi} \leftarrow -\frac{\xi_m}{2} [\sin(a_A (T - A_s) + b_A \sigma) + (a_A \dot{T} + b_A \dot{\sigma})]$$
4. Compute SMA strain rate upon heating:

$$\dot{\epsilon} \leftarrow \frac{\dot{\sigma} - \theta_s \dot{T} - \Omega \dot{\xi}}{E_A}$$
6. Integrate $\dot{\epsilon}$
7. Return ϵ

The step 1 computes the temperature rate (\dot{T}) based on the current input i . It allows for the evaluation of overheating when the SMAs are subject to high values of input power. The term m_{sma} is the mass of the wires, A_c is the circumferential area of the wire, c_p is the specific heat, R_{sma} is the electrical resistance and h_c is the heat coefficient.

During step 2 the stress rate $\dot{\sigma}$ is calculated. The equation allows us to observe stress effects caused by overheating the wires, thus identifying an upper threshold for the input current i . The term θ_s is the thermal expansion factor of the wire, Ω is the phase transformation factor, A_f, A_s are the Austenite border condition upon temperature and C_m is the stress coefficient. Based on that, the changes between transformation phases (hysteresis curve) are calculated during step 3, where $\dot{\xi}$ is the phase transformation rate that describes the phase transformation from martensite to austenite. Finally, step 4 calculates the SMA strain due to the contraction. More details on the model's parameters can be found in (Elahinia, 2005).

2.2 Exoskeleton's Equations of Motion

In Fig 1 we proposed a 2 Degree-of-Freedom (DoF) serial link model to represent the exoskeleton mechanics of the finger. Also, each finger is treated separately, as a branched of rigid bodies connected to the same fixed-based.

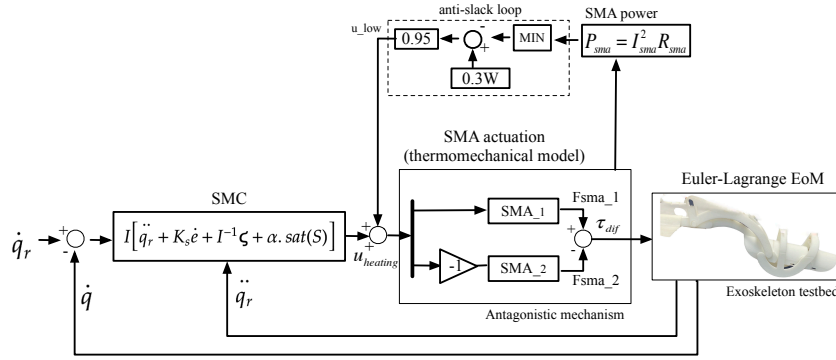


Figure 2: SMA control architecture.

The joint q_1 is directly driven by the SMA antagonistic pair of artificial muscles, while the joint q_2 is under-actuated, i.e. kinematically coupled to the former joint. Here, we apply the well-known Euler-Lagrange formalism to determine the corresponding Equations of Motion (EoM). First, we derive the velocities of each body, such as:

$$\begin{aligned} \dot{x}_1 &= -L_{c1} \sin(q_1) \dot{q}_1 \\ \dot{y}_1 &= L_{c1} \cos(q_1) \dot{q}_1 \\ \dot{x}_2 &= -L_1 \sin(q_1) \dot{q}_1 - L_{c2} \sin(q_1 + q_2) (\dot{q}_1 + \dot{q}_2) \\ \dot{y}_2 &= L_1 \cos(q_1) \dot{q}_1 - L_{c2} \cos(q_1 + q_2) (\dot{q}_1 + \dot{q}_2) \end{aligned} \quad (1)$$

where $[\dot{x}_1, \dot{y}_1]$ and $[\dot{x}_2, \dot{y}_2]$ describe the components of the center of mass velocity for each body of the exoskeleton, according to the diagram in Fig 1. Having the velocity, the kinetic energy can be calculated, while the potential energy is neglected, since gravity will be compensated by a closed-loop control law. In this regard, the Lagrangian operator (L) is defined as:

$$L(q, \dot{q}) = 0.5 [m_1 (L_{c1}^2 \dot{q}_1^2) + m_2 (L_1^2 \dot{q}_1^2 + L_{c2}^2 (\dot{q}_1 + \dot{q}_2)^2)] \quad (2)$$

Applying the Euler-Lagrange formulation, the state-variable EoM are defined as follows:

$$\begin{aligned} \dot{X}_1 &= X_2 \\ \dot{X}_2 &= \dot{q}_1 = \frac{\tau_1 - m_2 L_{c2}^2 \ddot{q}_2}{m_1 L_{c1}^2 + m_2 L_1^2 + m_2 L_{c2}^2} \\ \dot{X}_3 &= X_4 \\ \dot{X}_4 &= \dot{q}_2 = \frac{\tau_2 - m_2 L_{c2}^2 \ddot{q}_1}{m_2 L_{c2}^2} \end{aligned} \quad (3)$$

2.3 SMA Control

Figure 2 introduces the closed-loop control architecture for the exoskeleton. This control scheme is composed by three loops: i) an inner loop to feedback joint accelerations (\ddot{q}_r) based on the EoM defined in Eq. 3, ii) an outer loop to regulate the exoskeleton's angular position (q) or velocity (\dot{q}) according to the

rehabilitation reference trajectory, and iii) an upper loop in charge of supervising the SMA's power consumption (P_{sma}), as function of the measured electrical current (I_{sma}) and the known electrical resistance (R_{sma}) of the SMA wires.

As detailed in Fig 2, the input torques τ_1 and τ_2 are both functions of the generated pull-force driven by the SMA antagonistic mechanism, being $\tau_{dif} = F_{sma1} - F_{sma2}$. Thanks to the aforementioned upper loop, the SMA wires do not cool entirely, while maintaining a minimum threshold for the input current $i = u_{heating}$ injected by the control law. This setup avoids wire slack, while tacking advantage of the pseudo-elasticity phenomenon presented in NiTi alloys, resulting in a more precise operation of the antagonistic mechanism. Based on this, a non-linear control method based on the sliding-mode technique (SMC) is proposed as follows:

- A sliding surface of the form $S = \dot{e} + K'_s e$ defines the dynamics that governs the system behavior while sliding, with gain $K'_s > 0$.
- The SMC control law ($u_{heating}$) is designed according to a Lyapunov function of the form: $V = 0.5 S^T$, $S > 0$.
- The sliding control is chosen such as $\dot{V} = S^T \dot{S} < 0$, or $-\alpha S^T \text{sgn}(S)$.
- The sliding condition is $\dot{S} = -\alpha \text{sgn}(s)$.

By differentiating $S = \dot{e} + K'_s e$ with respect to time:

$$\dot{S} = \ddot{q}_r - \ddot{q} + K'_s \dot{e} \quad (4)$$

In Eq. (4) the term \ddot{q}_r represents the forward dynamics solution in canonical form:

$$\ddot{q}_r = [I^{-1} (F - \xi)], \quad (5)$$

where F is the applied force, ξ is the Coriolis term and I is the moments of inertia. By substituting Eq. (5) into (4):

$$\dot{S} = \ddot{q}_r - [I^{-1} (F - \xi)] + K'_s \dot{e} \quad (6)$$

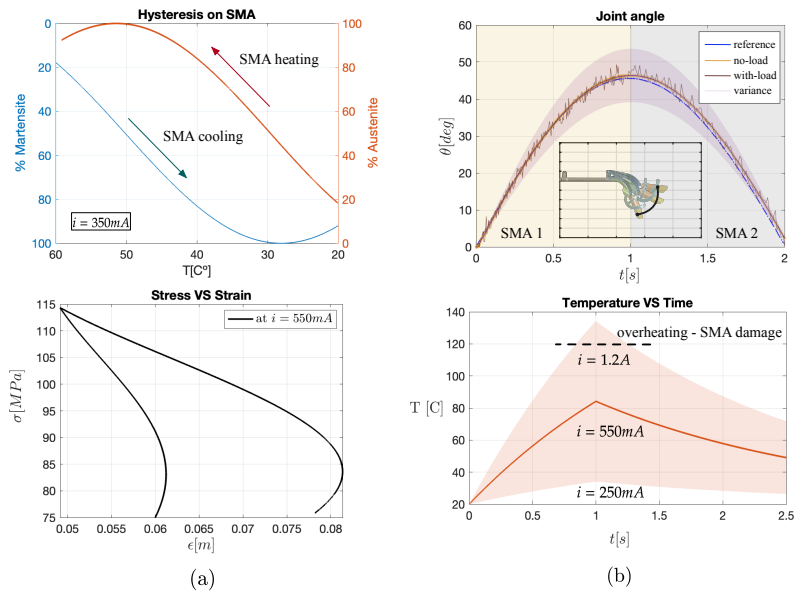


Figure 3: SMC-driven SMA actuation for joint position control. (a) Simulation results of SMA hysteresis, stress and strain by following the thermo-mechanical model described in Algorithm 1. (b) SMA-driven exoskeleton motion tracking by combining the dynamics model presented in Eq. 3 and the actuation law described in Eq. 8.

By equaling Eq. (6) with the sliding condition $\dot{S} = -\alpha \text{sgn}(s)$, and then isolating F , yields:

$$\begin{aligned} -\alpha \text{sgn}(s) &= \ddot{q}_r - [I^{-1}(F - \xi)] + K'_s \dot{e} \\ F &= I[\ddot{q}_r + K'_s \dot{e} + I^{-1}\xi + \alpha \text{sgn}(s)] \end{aligned} \quad (7)$$

By renaming $u_{\text{heating}} = F$, the sliding control law is derived from Eq. (7), as:

$$u_{\text{heating}} = I[\ddot{q}_r + K'_s \dot{e} + I^{-1}\xi + \alpha \text{sgn}(s)] \quad (8)$$

The control gains K'_s and α must be positive.

3 RESULTS

The results reported in this section are oriented to determine the limits of SMA operation. To this purpose, three operation modes for the SMA actuators were defined in terms of the driven electrical current injected by the SMC controller: i) low ($i = 250\text{mA}$), ii) nominal ($i = 550\text{mA}$), and iii) overheating ($i > 1200\text{mA}$).

Using Algorithm 1, thermo-mechanical equations are computed, in order to evaluate SMA stress, temperature, hysteresis, strain and the range of motion, according to the operations modes previously defined. Also, Table 1 summarizes the parameters used for the models.

Figure 3 presents the results of controlling the exoskeleton's tested by regulating joint positions. Plots 3(a) depict the transformation phases exhibited by the

Table 1: Parameters for SMA thermo-mechanical model.

Parameters	Values [unit]
m_{sma}, R_{sma}	$1.14 \times 10^{-4} [\text{Kg}], 8.5 [\Omega]$
A_c	$1.76 \times 10^{-8} [\text{m}^2]$
h_c	$150 [\text{Jm}^{-2}\text{C}^{-1}\text{s}^{-1}]$
C_p	$0.2 [\text{KcalKg}^{-1}\text{C}^{-1}]$
Ω	$-1.12 [\text{GPa}]$
θ_s	$0.55 [\text{MPa}^2\text{C}^{-1}]$
C_m, C_a	$10.3 [\text{MPa}^2\text{C}^{-1}]$
A_s, A_f, M_s, M_f	$68, 78, 52, 42 [\text{C}^\circ]$
E_A	$75 [\text{GPa}]$
E_M	$28 [\text{GPa}]$
ξ_m, ξ_a	$1, 0 [\text{dimensionless}]$
a_A	$0.31 [\text{C}^{-1}]$
a_M	$0.31 [\text{C}^{-1}]$
b_A, b_M	$-0.03 [\text{C}^{-1}]$

SMA actuator, including the stress and strain over the alloys during deformation upon heating. The results were obtained by applying the thermo-mechanical model described in Algorithm 1. We applied several input electrical currents to the SMA actuator, ranging from 250mA up to 1.2A . With these input parameters, the SMA actuator contracts from 1mm up to 4mm . As expected, the linear contraction of the muscle-like mechanism yields an angular motion ranging between 40 to 52 degrees in rotational motion, as shown by the upper plot of Fig 3(b). As mentioned, the SMC control law described in Eq. 8 injects power to the SMA pair of artificial muscles, where u_{heating} is the driven electrical current.

The lower plot of Fig 3(b) describes the alloy temperature range according to the input current for low,

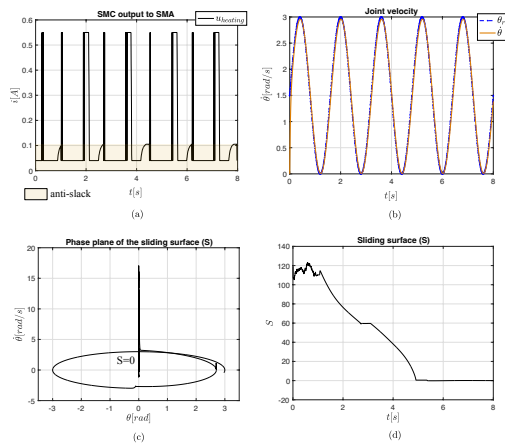


Figure 4: SMC-driven SMA actuation for joint velocity control.

nominal and overheating operation modes. As observed, applying a nominal value of $550mA$ to the SMA actuator allows the exoskeleton to follow the corresponding opening and closing gesture trajectory of reference. Note in the inset of the upper plot in 3(b), that the resultant range of motion corresponds to the fingertip cartesian point of the exoskeleton, whereas the antagonistic configuration is differentiated for each SMA actuator driving both open and close gestures independently.

Under this scenario, SMA contraction and extension is achieved in $2s$, with a maximum SMA strain of $4mm$. As observed, the SMC-based position controller is not achieving the expected accuracy and precision during the reference tracking, concretely for the opening gesture driven by the antagonistic pair (SMA 2). The inertial load cannot be counteracted with the position feedback, yielding larger tracking errors compared against the closing gesture driven by the SMA 1. This outcome could be associated to the fact that the control law in Eq. 8 was defined to smoothly regulate velocity references rather than positions, since the contraction rate of the SMA actuator is linearly dependant to the changes of the inner electrical resistance of the alloys.

In order to improve on tracking accuracy and precision, the reference trajectory was changed from angular position to velocity (as a function of the SMA contraction rate). Figure 4 presents the results. Plot 4(a) shows the electrical current ($u_{heating}$) applied to each SMA actuator. Thanks to the anti-slack upper-loop shown in Fig 2, note how the electrical current maintains a minimum threshold value of $50mA$, avoiding the SMA alloys of completely cooling after contraction, which increase bandwidth control and actuation frequency. Also, the term $u_{heating}$ was saturated to operate at a nominal value of $550mA$, avoid-

ing the limits of overheating at $> 1200mA$, since higher electrical currents will result in alloy temperatures $> 120^\circ C$, causing irreversible damage to the one-way shape memory effect.

Under this scenario, the SMC control law was able to properly regulate the joint velocity, maintaining a precise tracking of the trajectory, as depicted in plot 4(b). Controlling the contraction rate rather than the specific position of the SMA actuator allows the SMC method to smoothly track the desired motion, since the control law is strictly dependent on the dynamics model of the exoskeleton, as denoted by the term \ddot{q}_r in Eq. 8. This model-dependent controller counteracts the inertial loads more accurately, since the sliding surface $S = \dot{e} + K'_s e$, governs both the tracking error (e) and error dynamics rate \dot{e} . Plots 4(c,d) detail how the sliding surface goes to zero, fulfilling with the Lyapunov function condition.

4 CONCLUSIONS

We have demonstrated the feasibility of the use of muscle-like SMA actuators for the soft control of the exoskeleton testbed presented in Fig 1. A comprehensive thermo-mechanical model for NiTi SMA wires allowed us to analyze the limits of this actuation technology in terms of power consumption, control bandwidth, and motion range. The SMA actuator can operate with input electrical currents ranging from $250mA$ up to $1.2A$ and generating an output motion range from 40 to 52 degrees in rotation, which coincides with the average range of motion of a normal grip movement at the metacarpophalangeal (MP) joint with an average of 44 degrees (Shimawaki, 2019). Unfortunately, this outcome still does not work to achieve full opening and closing of the hand, since the SMA alloys exhibited a maximum stroke of $4mm$. We need to increase the contraction length of the wires, by adding artificial tendons connecting the SMA muscles directly to both joints, specially to the second joint (q_2) of the exoskeleton.

In terms of control bandwidth, we achieved an actuation frequency of $1.5Hz$, being sufficient to further assist the patient according to the rehabilitation gestures. Furthermore, the proposed sliding-mode control technique (SMC) obtained accurate results in tracking the desired angular velocity, mostly due to the incorporation of the exoskeleton inertial model contained in the terms I and \ddot{q}_r of Eq. 8, allowing the SMC controller to counteract the loads more precise and smooth. Overall, we believe that the actuation based on SMAs could be an alternative in robotic-assisted rehabilitation of the hand. Upcoming work

is oriented towards the measurement and characterization of the SMA pull-force, in order to determine the maximum loads supported by the soft actuation mechanism presented herein.

ACKNOWLEDGEMENTS

This work was funded by the project “iREHAB: Sistema inteligente de Rehabilitación usando un Exoesqueleto para recuperar Habilidad motora en discapacidades post-ACV, usando señales Biológicas del paciente” sponsored by The Ministry of Science Technology and Innovation (MinCiencias), program 918-2022 under GRANT CTO: 622-2022, Award ID: 91805.

REFERENCES

- A. K. Mishra, V. S. Janani Kavi Priya, K. Pradeep, J. Sai Vaishnav, and G. Kabhilesh, “Smart materials for ultrasonic piezoelectric composite transducer: A short review,” *Mater Today Proc*, vol. 62, pp. 2064–2069, Jan. 2022, doi: 10.1016/j.matpr.2022.02.514
- M. Hodgins, G. Rizzello, D. Naso, A. York, and S. Se-elecke, “An electro-mechanically coupled model for the dynamic behavior of a dielectric electro-active polymer actuator,” *Smart Mater Struct*, vol. 23, no. 10, Oct. 2014, doi: 10.1088/0964-1726/23/10/104006
- Z. Guo, Y. Pan, L. B. Wee, and H. Yu, “Design and control of a novel compliant differential shape memory alloy actuator,” *Sens Actuators A Phys*, vol. 225, pp. 71–80, Apr. 2015, doi: 10.1016/j.sna.2015.01.016.
- N. Bhatt, S. Soni, and A. Singla, “Analyzing the effect of parametric variations on the performance of antagonistic SMA spring actuator,” *Mater Today Commun*, vol. 31, Jun. 2022, doi: 10.1016/j.mtcomm.2022.103728.
- H. Jeong and W. D. Wang, “Self-adaptive detachable pneumatic soft actuators using uniformly distributed temporary-bonding-fasteners for wearable applications,” *Sens Actuators A Phys*, vol. 349, Jan. 2023, doi: 10.1016/j.sna.2022.114083.
- H. Jin, E. Dong, M. Xu, C. Liu, G. Alici, and Y. Jie, “Soft and smart modular structures actuated by shape memory alloy (SMA) wires as tentacles of soft robots,” *Smart Mater Struct*, vol. 25, no. 8, Jul. 2016, doi: 10.1088/0964-1726/25/8/085026.
- G. Stano and G. Percoco, “Additive manufacturing aimed to soft robots fabrication: A review,” *Extreme Mechanics Letters*, vol. 42, Elsevier Ltd, Jan. 01, 2021. doi: 10.1016/j.eml.2020.101079.
- Y. Wang, S. Zheng, Z. Song, J. Pang, and J. Li, “A Coupling Dynamic Model for Studying the Physical Interaction between a Finger Exoskeleton and a Human Finger,” *IEEE Access*, vol. 8, pp. 125412–125422, 2020, doi: 10.1109/ACCESS.2020.3007799.
- Ruth, D.J.S.; Sohn, J.-W.; Dhanalakshmi, K.; Choi, S.-B. Control Aspects of Shape Memory Alloys in Robotics Applications: A Review over the Last Decade. *Sensors* 2022, 22, 4860. <https://doi.org/10.3390/s22134860>
- D. Singh, R. Choudhury, M. Mukherjee, and Y. Singh, “Development of non-linear models to evaluate the NiTi SMA spring actuator”, *JMES*, vol. 16, no. 1, pp. 8754–8769, Mar. 2022.
- Abdul Manan Khan, Youngshik Kim, Buhyun Shin, Mahyar Hasanzadeh Moghadam, Nader A. Mansour, Modeling and control analysis of an arc-shaped SMA actuator using PID, sliding and integral sliding mode controllers, *Sensors and Actuators A: Physical*, Vol 340, 2022, 113523.
- Castiblanco, J.C.; Mondragon, I.F.; Alvarado-Rojas, C.; Colorado, J.D. Assist As Needed Exoskeleton for Hand Joint Rehabilitation Based on Muscle Effort Detection. *Sensors* 2021, 21, 4372. <https://doi.org/10.3390/s21134372>
- K. Zuo, B. Wang, and Y. Wang, “Research on exoskeleton structure design of hand function rehabilitation robot,” in *2022 12th International Conference on CYBER Technology in Automation, Control, and Intelligent Systems, CYBER 2022*, 2022, pp. 812–816. doi: 10.1109/CYBER55403.2022.9907104.
- Mohammad H Elahinia and Mehdi Ahmadian 2005. An enhanced SMA phenomenological model: I. The shortcomings of the existing models. *Smart Mater. Struct.* 14 1297, 10.1088/0964-1726/14/6/022
- Tanaka K 1986 A thermomechanical sketch of shape memory effect: one-dimensional tensile behavior *Res. Mech., Int. J. Struct. Mach. Mater. Sci.* 18 251-63.
- Shimawaki, S., Murai, T., Nakabayashi, M., Sugimoto, H. (2019). Measurement of flexion angle of the finger joint during cylinder gripping using a three-dimensional bone model built by X-ray computed tomography. *Applied bionics and biomechanics*, 2019.
- Colorado J. (2012). BaTboT: a biologically inspired flapping and morphing bat robot actuated by SMA-based artificial muscles. Thesis (Doctoral), E.T.S.I. Industriales (UPM). <https://doi.org/10.20868/UPM.thesis.14657>.
- W. Coral, C. Rossi, J. Colorado, D. Lemus, and A. Barrientos, SMA-Based Muscle-Like Actuation in Biologically Inspired Robots: A State of the Art Review, *Smart Actuation and Sensing Systems - Recent Advances and Future Challenges*, Oct. 2012, doi: 10.5772/50209.